Electrical properties of $Ni_{1-x}Co_xS_2$

A. K. Mabatah,*† Ellen J. Yoffa,*‡ P. C. Eklund,§‖ M. S. Dresselhaus,§ and David Adler§
Center for Materials Science and Engineering, Massachusetts Institute of Technology, Cambridge, Massachusetts 02139
(Received 26 June 1978)

We report results of electrical-conductivity, thermoelectric-power, and optical experiments on single crystals of $Ni_{1-x}Co_xS_2$ ($0 \leq x \leq 0.12$). The results cannot be explained by means of a conventional one-electron model. However, if it is assumed that both strong electronic correlations and strong electron-phonon coupling exists for electrons in the narrow d bands associated with the transition-metal cations, the experimental results can be understood quantitatively. In the model presented, NiS_2 is a Mott insulator, in which the gap is due to a correlation splitting of the $3d$-e_g band. The introduction of Co substitutionally for Ni results in one hole per Co atom in the lower of these bands. However, strong electron-phonon coupling leads to small-polaron formation, and thus a drastic band narrowing with increasing temperature. For this range of x, the d-band holes conduct only by means of thermally activated hopping for temperatures above 100 K. Screening effects due to thermally excited carriers lead to a collapse of the energy gap at a critical temperature, but small-polaron hopping remains the predominant conduction mechanism.

I. INTRODUCTION

Ever since the pioneering work of Bither *et al.*,[1] the pyrite-structure transition-metal dichalcogenides have been intensively studied.[2-12] The electronic properties of these materials are thought to be controlled by the $3d$-e_g band of the transition-metal cations.[1-3,5-6] This band contains four states per cation. Thus, in the disulfides, for example, FeS_2 has an empty e_g band and ZnS_2 has a filled e_g band and both are insulators; on the other hand, CoS_2 and CuS_2 have one-quarter- and three-quarter-filled bands, respectively, and both are metallic. From this viewpoint, the most interesting pure material is NiS_2, which should have a half-filled e_g band, but is nevertheless semiconducting. This apparent breakdown of the one-electron model led to the initial suggestion that NiS_2 is a Mott insulator,[2] nonmetallic only as a result of strong correlations among the e_g electrons.[13] Some supporting evidence for this is the fact that NiS_2 undergoes a semiconductor-metal transition at a pressure of about 30 kbar,[7,9] but previous optical-absorption, electrical-conductivity, and thermoelectric-power data have also been interpreted by assuming that the material is a partially compensated wide-band semiconductor.[8] Thus, it has not been clear whether or not NiS_2 is a Mott insulator.

Some insight into the question can be gained by alloying NiS_2 with either CoS_2 or CuS_2, thus respectively either decreasing or increasing the number of electrons in the e_g band. This procedure is analogous to ordinary semiconductor doping, in that it creates either holes in the valence band or electrons in the conduction band. Several investigations of the $Ni_{1-x}Co_xS_2$ and $Ni_{1-z}Cu_zS_2$ systems have shown that the semiconducting behavior is maintained at least up to $x \approx 0.07$ and $z \approx 0.05$.[4] In addition, in sulfur-deficient compounds $NiS_{2-\delta}$, the semiconductivity is maintained up to $\delta \approx 0.09$,[10] but the critical pressure for the semiconductor-metal transition decreases rapidly with nonstoichiometry.[11] None of the previous investigators proposed any quantitative model to explain their data.

To gain insight as to whether NiS_2 is a Mott insulator, we have measured systematically several transport properties of well-characterized $Ni_{1-x}Co_xS_2$ samples in the semiconducting phase, $0 \leq x \leq 0.12$. We report here results of measurements of the electrical conductivity and thermoelectric power of such single crystals, and present a model which quantitatively explains the observed temperature and composition dependence. The excellent fit that is obtained strongly suggests that NiS_2 is a Mott insulator in which transport occurs predominantly by the phonon-assisted hopping of small polarons. A preliminary account of this study has been described elsewhere.[14]

In Sec. II, we describe the experimental techniques employed in our investigations. The effects of impurities and nonstoichiometry on the electrical conductivity and thermoelectric power were studied explicitly. Because the Hall effect in these materials was found to be quite small and was not measurable with our experimental apparatus, a careful study of the thermoelectric power became necessary to obtain quantitative information about the temperature dependence of the carrier concentration. The electrical conductivity and thermoelectric power measurements on single crystals of $Ni_{1-x}Co_xS_2$ for $0 \leq x \leq 0.12$ are presented in Sec. III. The results cannot be consistently explained using conventional one-electron theory. Instead, we develop a the-

oretical model which invokes both strong electronic correlations and strong electron-phonon coupling. The model is described in Sec. IV and the fit to our experimental results is discussed in Sec. V. Since the fit requires that the energy gap of $Ni_{1-x}Co_xS_2$ decreases with increasing temperature, optical absorption and reflectivity measurements on selected samples were performed, and these optical results are also discussed in Sec. V. General conclusions are presented in Sec. VI.

II. EXPERIMENTAL DETAILS

A. Sample preparation

Single crystals were grown by a chemical-vapor-transport technique.[15] The method consisted of two steps: (i) preparation of polycrystalline starting materials, and (ii) growth of single crystals. For NiS_2, the reagent materials were specpure nickel and sulfur powders,[16] and polycrystalline samples of $Ni_{1-x}Co_xS_2$ were prepared from analyzed nickel sulfate and cobalt sulfate solutions,[17] using the technique of Bouchard.[18] The use of the liquid sulfate solutions as starting reagents in the preparation of the polycrystalline alloy material is necessary to obtain sample homogeneity. Chlorine was used as the transport gas for NiS_2, but since bromine was found to give better crystal-growth results for the $Ni_{1-x}Co_xS_2$ system for $x>0$,[19] it was used for the alloys. Otherwise, crystal growth by the transport method was the same for both NiS_2 and $Ni_{1-x}Co_xS_2$ with $x>0$.

B. Sample characterization

The $Ni_{1-x}Co_xS_2$ crystals used in this study are listed in Table I. The largest single crystals of NiS_2 were about $4\times2\times2$ mm, and the size of the crystals decreased with increasing cobalt concentration. The facets of the crystals were generally well formed and many showed shiny surfaces. In the alloy samples, homogeneity is an important consideration. Electron-microprobe analysis showed that the samples used in this study were homogeneous to within 0.03% of x.

The cobalt concentration and sample stoichiometry were determined from x-ray lattice constant measurements, x-ray fluorescence measurements, and chemical analysis.[20] X-ray powder patterns confirmed the pyrite structure for all the specimens used in this study. Because of the variation of lattice constant with cobalt concentration,[18] accurate lattice constant determination was made from slow-scan x-ray powder diffraction patterns taken on a Norelco diffractometer [back reflection from 165° to 120° (2θ)] at room temperature. Copper radiation was employed and a silicon standard was used to calibrate the diffractometer. The lattice constants for the various samples are listed in Table I. The relation of lattice constant to x was obtained using the results of x-ray $K\alpha$ fluorescence measurements from both Ni and Co to determine their concentrations. The sulfur concentrations were determined by first dissolving the samples, adding $BaCl_2$, and then weighing the sulfur as the precipitate $BaSO_4$. These measurements determined the stoichiometry n and the cobalt concentration x, given in Table I. This information is summarized as the open circles in Fig. 1, which agree well with the triangles of Ref. 18. Most of the specimens, including NiS_2, were found to be sulfur rich by at least two percent, while the Co concentrations were found to deviate by $<0.5\%$ from the nominal Co composition of the polycrystalline alloy.

C. Electrical-conductivity and Hall-effect measurements

Conductivity measurements were made for the temperature range $100<T<600$ K using a Van der Pauw[21] technique appropriately modified for the various temperature ranges of interest to the present study. For the low-temperature ($T<300$ K) measurements, ohmic contacts were bonded on the sample by using conductive silver paint. For the high-temperature ($T>300$ K) measurements, Pt pressure electrodes and spot-welded leads (0.3 mm in diameter) were applied to the edges of the sample, and the sample chamber was continuously flushed with argon gas. The uncertainties[21] in the absolute accuracy of the resistivity measurements were about 5%, since the contact area was approximately 0.04 mm^2, while the sample area was typically 2 mm^2.

Hall-effect measurements were made for the temperature range $100<T<300$ K, in magnetic fields[22] of up to 150 kG, using a modified Van der Pauw technique.[23] This involved use of an external variable resistor in parallel with the sam-

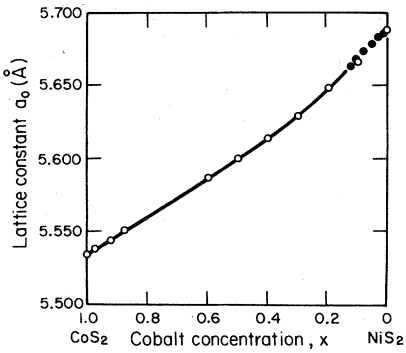

FIG. 1. Lattice constant a_0 of $Ni_{1-x}Co_xS_2$ vs x. The data represented by open circles are from Ref. 18 and by the closed circles from the present study.

TABLE I. Lattice constant and stoichiometry n of samples $Ni_{1-x}Co_xS_n$.

Nominal composition	Lattice constant (Å)	n	x
NiS_2	5.6879	2.06 ± 0.03	0.0
$Ni_{0.999}Co_{0.001}S_2$	5.6879	2.03 ± 0.03	0.001
$Ni_{0.995}Co_{0.005}S_2$	5.6872	2.03 ± 0.03	0.005
$Ni_{0.99}Co_{0.01}S_2$	5.6860	1.99 ± 0.03	0.01
$Ni_{0.98}Co_{0.02}S_2$	5.6845	2.07 ± 0.03	0.02
$Ni_{0.97}Co_{0.03}S_2$	5.6838	2.07 ± 0.03	0.03
$Ni_{0.95}Co_{0.05}S_2$	5.6785	2.07 ± 0.03	0.05
$Ni_{0.92}Co_{0.08}S_2$	5.6737	2.05 ± 0.03	0.08
$Ni_{0.90}Co_{0.10}S_2$	5.6687	2.06 ± 0.03	0.10
$Ni_{0.88}Co_{0.12}S_2$	5.6632	2.02 ± 0.03	0.12

ple to cancel out the offset voltage. This offset voltage arose because the electrodes were not on the same equipotential surface before the magnetic field was applied. Voltage measurements were accurate to 1 μV.

D. Thermoelectric-power measurements

For thermoelectric-power measurements in the temperature range $80<T<600$ K we have used a heat-pulse technique[24] which is particularly well suited to this temperature range and sample size. The error in the thermoelectric power measurement was $\leq 1\%$ over the entire temperature range.

E. Optical-absorption and reflectivity measurements

Optical-absorption and reflectivity measurements in the energy range $0.12<\hbar\omega<2$ eV were made using a Perkin-Elmer Model 112 double-pass prism monochromator. Because of the small size of the samples (~2×2 mm surface area), it was necessary to modify the usual detection arrangement, by introduction of an additional spherical mirror to focus the light beam on the sample. In addition, measurements in the energy range $0.06<\hbar\omega<0.4$ eV were made using a double-beam Fourier spectrometer.

The samples used for the absorption measurements were thin slices cut from single crystals with a string saw. Both sides of each slice were lapped with 2-μm polishing grit to produce a flat plate of thickness of about 40 μm, and then polished using Linde A polishing powder on a microcloth, to a thickness of ~25 μm. Since such thin samples were very fragile, the samples were attached with a thin film of vacuum grease[25] to thin BaF_2 substrates. For the reflectivity measurements, the samples were lapped down to 1-mm thickness using 2-μm polishing grit. Then, one of the surfaces was polished using Linde A grit on microcloth followed by Linde B and finally etched with 0.5% Chlorox solution on a supreme pad.

Measurements at temperatures $T<300$ K were made with the sample in an optical small cold-finger Dewar. Although the temperature was not measured, it was assumed to be within 5 °C of the liquid-nitrogen or dry-ice refrigerants within the Dewar.

III. EXPERIMENTAL RESULTS

Here we present the results of electrical-conductivity, Hall-effect, and thermoelectric-power measurements. These yield the temperature and concentration dependence of the carrier concentration and mobility, which will subsequently be explained in terms of a theoretical model to be described in Sec. IV. The results of the optical absorption and reflectivity measurements are presented in Sec. V to support some aspects of the theoretical model.

The electrical conductivity and thermoelectric power of the samples of $Ni_{1-x}Co_xS_2$, $0\leq x\leq 0.12$, exhibit a complicated temperature dependence. It is convenient to describe these properties with respect to five temperature regimes common to each x and the onset of which changes progressively with x.

A. Electrical conductivity

The results of the conductivity measurements made on $Ni_{1-x}Co_xS_2$, $0\leq x\leq 0.12$, are shown in Figs. 2–5.

Our results for undoped NiS_2, shown in Fig. 2, can be described by three distinct activation energies E_i ($i=0, 1, 2$); the other two temperature regimes would occur for $T>600$ K in this material. These results are in qualitative agreement with results of Kautz *et al.*[8] In the three temperature ranges $T>380$ K, $140\lesssim T\lesssim 380$ K, and $80\lesssim T\lesssim 140$ K, the activation energies for the NiS_2 in Fig. 2 are, respectively, $E_2=285$ meV, $E_1=59$ meV, and $E_0=12$ meV in comparison with the values of 320, 68, and 0.45 meV reported by Kautz *et al.* The discrepancy in the values for E_0 is due to the fact

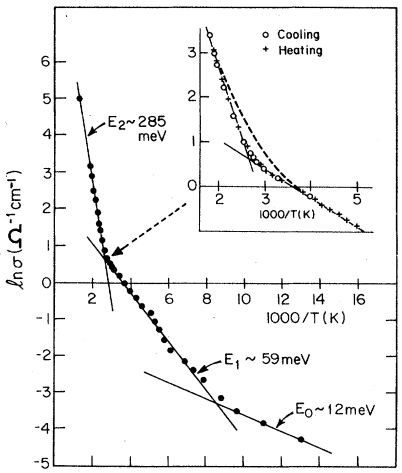

FIG. 2. Natural log of conductivity vs inverse temperature for NiS_2. The activation energies E_0, E_1, and E_2 for three temperature regimes are indicated. The inset shows that the experimental data for $T \simeq 380$ K cannot be fit by the superposition of two exponential terms corresponding to activation energies E_1 and E_2 (shown by the dashed curve).

that it is not a well-defined activation energy but rather varies with temperature; the value reported by Kautz *et al.* was based on measurements at $T<80$ K. As we shall discuss later, conductivity in this region is due to multiple-phonon hopping processes, and E_0 is thus not a significant parameter.

The kink in the NiS_2 conductivity curve at 380 K requires close attention. As shown in the inset

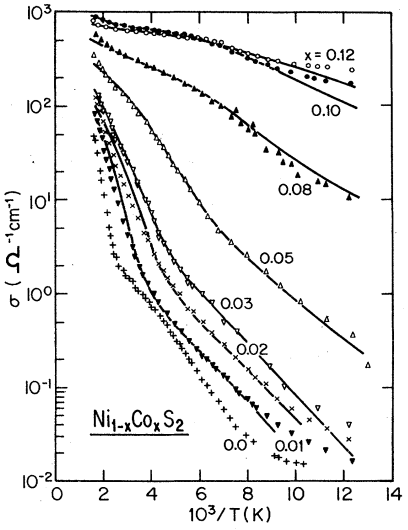

FIG. 3. Conductivity vs inverse temperature for $Ni_{1-x}Co_xS_2$ for various values of x. The experimental data are shown using the various symbols as indicated and the solid lines are theoretical fits (discussed in Sec. V A).

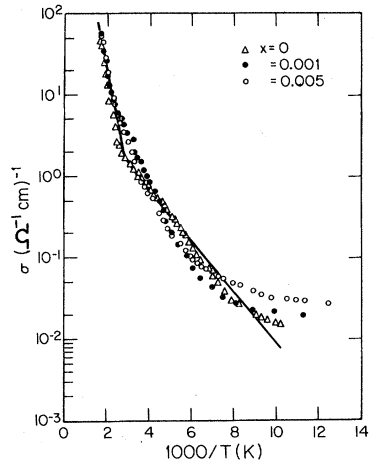

FIG. 4. Conductivity vs inverse temperature for $Ni_{1-x}Co_xS_2$, $x=0$, 0.001, and 0.005. The solid curve represents the fit to the data discussed in Sec. V A.

of Fig. 2, the experimental conductivity data in the region of the kink are not quantitatively described by that derived from a conventional two-band conduction model (dashed curve),[8] where the total conductivity, σ_t is given by summing the contributions for each band:

$$\sigma_t = \sigma_{01}e^{-E_1/kT} + \sigma_{02}e^{-E_2/kT}, \quad (1)$$

in which σ_{0i} and E_i, $i=1,2$ are, respectively, the infinite-temperature conductivities and activation energies due to band i.

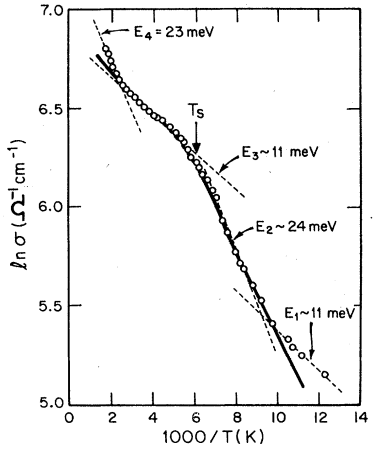

FIG. 5. Natural log of conductivity vs inverse temperature for $Ni_{0.90}Co_{0.10}S_2$. The experimental data are represented by circles. Results from the theoretical model (Sec. V A) are shown as a solid curve. T_s is the saturation temperature, above which the activation energy decreases to its smaller high-temperature value E_3. It is of interest that the high- and low-temperature activation energies E_1 and E_3 are equal and smaller than E_2.

The failure of this simple model suggests that NiS_2 might undergo a phase transition at approximately 380 K. Structural studies using high-temperature x-ray powder diffraction showed that for NiS_2 there was no lattice-constant discontinuity with temperature in the region around 380 K. On the other hand, an x-ray study by Furuseth *et al.*[26] indicated an anomaly in the thermal expansion of NiS_2 between 420 and 450 K. However, it should be noted that these workers could not detect this anomaly by differential thermal analysis. This later result has been confirmed by Honig.[27] Thus, the evidence for a phase transition in NiS_2 at 380 K is inconclusive.

For $0 \leq x \leq 0.12$, the representative set of conductivity curves is shown in Fig. 3. These results confirm the existence of an activated conductivity, as first reported by Ogawa *et al.*[4] However, our $Ni_{0.88}Co_{0.12}S_2$ single crystals also exhibit semiconducting properties in the temperature range of $100 < T < 600$ K, contrary to what was observed previously in polycrystalline samples.[4] The thermally activated conductivities, σ in Fig. 3, tend to a common maximum of $\sim 10^3\ \Omega^{-1}\ \mathrm{cm}^{-1}$ at high temperatures. The activation energies and the total range of σ values decrease with increasing x for $0.01 \leq x \leq 0.12$ (see Fig. 3 and Table II). The results for $0 \leq x \leq 0.03$ are similar in features to those of NiS_2, as discussed above, and the three distinct activation energies E_i, $i = 0, 1, 2$ are listed in Table II. For higher values of x, $0.05 \leq x \leq 0.12$, σ exhibits some very unusual features, as illustrated in Fig. 5, for $x = 0.10$. For each value of x in the range $0.05 \leq x \leq 0.12$, $\sigma(T)$ may be described by four temperature regions including two new regimes of activation energies E_4 and E_3 (see Fig. 5). The regimes of activation energies E_2 and E_1 shift to lower temperatures, and E_0 shifts to $T < 77$ K. In the low- and high-T regions, the activation energies are equal ($E_1 = E_3$), while at intermediate temperatures, the activation energy is E_2, where $E_2 > E_1, E_3$. The "saturation" temperature T_s (defined as the temperature above which the activation energy decreases to its smaller, high-temperature value) is a decreasing function of cobalt concentration (see Table II). At high temperatures ($T \geq 500$ K), the conductivity activation energy (E_4) again increases (see Table II).

TABLE II. Conductivity activation energies E_i and saturation temperatures T_s for $Ni_{1-x}Co_xS_2$ vs x for $0 \leq x \leq 0.12$. E_0, E_1, E_2, E_3, and E_4 are the activation energies at very low, low, intermediate, high, and very high temperatures, respectively. The conductivity data for $x \leq 0.03$ do not exhibit any saturation feature (see Sec. III A).

x	E_0 (meV)	E_1 (meV)	E_2 (meV)	E_3 (meV)	E_4 (meV)	T_s (K)
0.0	12	59	285			
0.001	5	100	283			
0.005	8	65	265			
0.01	24	52	213			
0.02	25	53	165			
0.03	28	50	136			
0.05		43	77	43	130	240
0.08		22	44	22	50	180
0.10		11	24	11	22	165
0.12		8	19	8	23	155

Figure 4 shows that the conductivity curves for the samples $x = 0$, 0.001, and 0.005 are very similar, suggesting that at such low concentrations, the cobalt dopant is not the dominant effect and the presence of other impurities and nonstoichiometry such as Ni vacancies (see Sec. II B) must be considered. The curves deviate from the nearly common values only at low temperatures, where we expect the precise amount and nature of these defects to become important. Thermoelectric-power measurements, to be discussed later, also indicate that at such small x values, the electronic processes are no longer controlled primarily by Co concentration.

B. Hall effect

Hall-effect measurements would be significant for this work because the Hall constant together with the electrical conductivity could be used to separate the variation of the carrier concentration from that of the mobility. Unfortunately, the Hall voltage V_H for these materials is smaller than our experimentally detectable limit of 2 μV. Since $V_H < 2\ \mu$V, we obtain an upper limit of 0.5 $\mathrm{cm}^2/\mathrm{V\,sec}$ for the Hall mobility over the temperature and magnetic-field ranges $100 < T < 300$ K and $0 < B < 150$ kG.

C. Thermoelectric power

The results of the thermoelectric-power measurements on $Ni_{1-x}Co_xS_2$ may be described in terms of three principal temperature regimes: These low-, intermediate-, and high-temperature regimes correspond to those of conductivity activation energies E_0 and E_1, E_2, and E_3 and E_4, respectively. In Figs. 6, 7, and 8, we show the results of the thermoelectric-power measurements as functions of x and temperature for $0.0 \leq x \leq 0.12$, $0 \leq x \leq 0.005$, and $x = 0.10$, respectively. For samples with $0.005 \leq x \leq 0.01$ (see Figs. 6 and 7), the thermoelectric power S increases with increasing temperature from a small positive value near 80 K, to a large, positive maximum at intermediate temperatures, and then it decreases to a relatively small, negative and *temperature-independent* value at high temperatures. The magnitude and

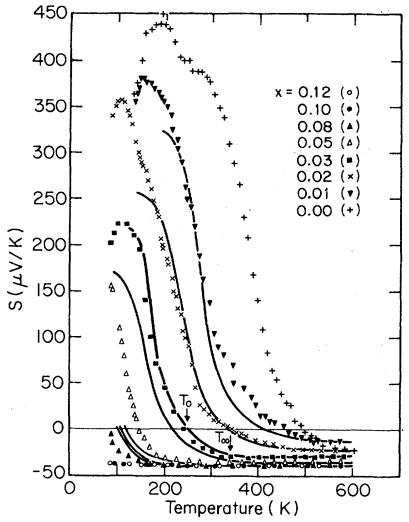

FIG. 6. Thermoelectric power S vs temperature for $Ni_{1-x}Co_xS_2$ for various values of x. The experimental data are shown using the various symbols as indicated and the solid curves represent theoretical fits as discussed in Sec. V B. T_0 is the cross-over temperature at which the experimental S changes sign and T_∞ is the onset temperature where S becomes temperature independent (indicated for $x = 0.03$).

location of the peak in S, the temperature T_0 at which S changes sign, and the onset temperature T_∞ for temperature-independent behavior (see Fig. 9) all decrease with increasing x. In the range $0.05 \leq x \leq 0.12$ and at $T > 160$ K, the thermoelectric power is negative (with a maximum saturation magnitude of ~ -40 μV/K) and temperature independent. Indeed, the thermoelectric powers of samples with $x = 0.10$ and 0.12 are temperature independent for the entire measured range of temperature, $80 < T < 600$ K (see Fig. 8).

For $0.0 \leq x \leq 0.005$ (see Fig. 7) the thermoelectric-power peaks and cross-over temperatures do not vary with x in a clear manner. This indicates, consistent with the conductivity data, that for such values of x, the cobalt dopant is not the dominant impurity. The thermoelectric powers for $x = 0.0$ and $x = 0.001$ do not show a temperature-independent region in the range of high temperatures that was experimentally accessible; we were unable to investigate the possibility that $T_\infty > 650$ K for these samples, due to the fact that they decompose when heated to such temperatures.[28] It is of interest, however, that the thermoelectric power of NiS_2 does not show any unusual behavior in the vicinity of 380 K, in contrast to the behavior of σ in that range of T (see Fig. 2). Our results for undoped NiS_2 in the temperature range $300 \leq T \leq 600$ K agree with those reported by Kautz *et al.*[8]

The possibility that the $x = 0.0$ and 0.001 samples exhibit a temperature-independent thermoelectric power at very high temperatures is supported by Fig. 9, which shows that upon extrapolation for

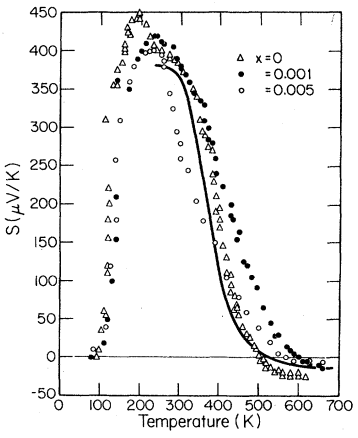

FIG. 7. Thermoelectric power vs temperature for $Ni_{1-x}Co_xS_2$, $x = 0$, 0.001, 0.005. The solid curve represents the fit to the data discussed in Sec. V B.

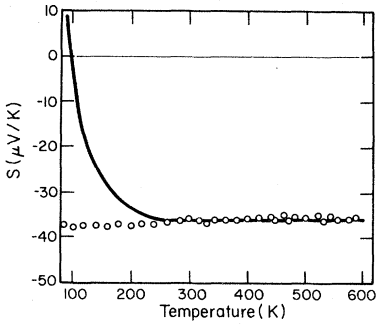

FIG. 8. Thermoelectric power S vs temperature for $Ni_{0.90}Co_{0.10}S_2$. The experimental data are represented by the open circles and the results of the theoretical fit (Sec. V B) by the solid curve.

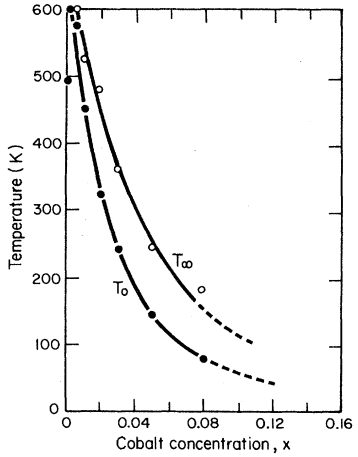

FIG. 9. Crossover temperature T_0 and the onset-temperature T_∞ of the temperature-independent behavior of S vs. x.

$x<0.005$, a value of $T_\infty>600$ K is obtained. This figure also shows that the high-temperature regime extends to lower temperatures with increasing x and that for $0.08<x\leq0.12$, extrapolation of the data suggests that S should become positive at low T, $40\lesssim T_0<80$ K.

The values of the temperature-independent thermoelectric power S_∞, observed at high T for samples with $0.005\leq x\leq0.12$, have been plotted as a function of x in Fig. 10. We find that at 600 K, which is in the high-temperature regime for this entire concentration range, S_∞ increases with x from -9 μV/K for $x=0.005$ to -38 μV/K for $x=0.05$, and then remains approximately independent of x ($0.05<x\leq0.12$) at -38 μV/K.

It is clear from these results that some interesting and anomalous transport properties characterize these materials. It can be shown[23] that one cannot explain these anomalous features using the conventional one-electron band model of Kautz *et al.*[8] or even several modified versions of this model still within the uncorrelated one-electron picture. The particular features which cannot be explained are as follows: the complicated dependence of the conductivity activation energies on x; for $0.05\leq x\leq0.12$ the activation energies at low and high temperatures are equal and less than that at intermediate temperatures. In addition, in the high-temperature regime, the thermoelectric power is temperature-independent. However, in the following we present a model for the $Ni_{1-x}Co_xS_2$ system, based on electron correlations in a narrow band, that explains quantitatively the transport properties discussed above.

IV. DISCUSSION

A. Model for $Ni_{1-x}Co_xS_2$ transport properties

The main features of the model discussed here are due to strong interelectronic correlations and electron-phonon interactions. In agreement with the suggestions of other workers[4,6,7,10], we assume that the energy band relevant to transport in the $Ni_{1-x}Co_xS_2$ system, the $3d$-e_g band, is narrow and split in two by strong interelectronic correlations, with correlation energy U. In pure stoichiometric NiS_2, the lower band is exactly full, and the upper band is empty, so that NiS_2 is a semiconductor. The e_g levels are well separated from a lower filled t_{2g} band and a higher-energy empty antibonding band.[1,3]

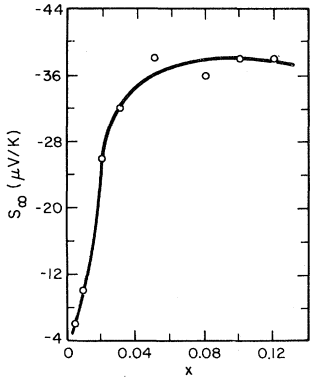

FIG. 10. Thermoelectric power S_∞ at $T=600$ K vs cobalt concentration x.

For $Ni_{1-x}Co_xS_2$ samples with $x>0$, Co enters the lattice substitutionally[3] for Ni, and hence does not markedly perturb the crystal structure. As a result, we assume that the energy-level scheme does not change appreciably for small Co concentrations. However, since Co^{2+} has one fewer electron than Ni^{2+}, the addition of Co continuously changes the occupancy of the lower band. Theoretical band calculations for FeS_2,[29] and photo-electron spectroscopy measurements,[30] both suggest that the e_g bandwidth is of the order of 1.0 eV. However, this does not take into account the band narrowing that results from small-polaron formation. Holstein[31] has shown that the bandwidth at zero temperature is reduced from that calculated from a rigid lattice approximation by a factor of $\exp(-S_0)$, where S_0 is the ratio of the polaron binding energy to the optical phonon energy. This could well reduce the bandwidth in NiS_2 by a factor of more than 100. Similar effects are known to drastically reduce the effective $3d$ bandwidth in materials such as NiO.[32] In addition, our Hall-effect measurements indicate that the *transport* properties of NiS_2 can be characterized by electrons with a large effective mass moving in a narrow band. Such large effective masses are almost certainly due to the formation of small polarons. We have thus assumed in our model that conduction within these correlation-split bands in $Ni_{1-x}Co_xS_2$ is dominated by phonon-assisted hopping.

In order to simplify the calculations, we have assumed that the effective bandwidth Δ is small ($\Delta\ll U, \Delta\ll kT$). Of course, this assumption must become invalid at a sufficiently low temperature, before the polaron band-narrowing effects are decisive. As we shall demonstrate, our simple model is able to explain the experimental results quantitatively down to about 100 K. Below this temperature, the observed behavior begins to depart from that predicted by the model. In the very low temperature regime, the transport data suggest that the variation of the occupation numbers with energy within the band becomes important. We also assume that the temperature dependence of the energy gap is given by $U(T)=U_0-\gamma kT$, where U_0 is the gap at $T=0$ and γ is a constant. We have shown[33] that a temperature-induced col-

lapse of the gap results from screening of the correlation energy by excited carriers. It was demonstrated that unless the bandwidth is sufficiently small, this gap collapse occurs abruptly. The present experimental results indicate only a gradual decrease in the size of the gap, and hence provide further support for the assumption of a narrow e_g bandwidth for the $Ni_{1-x}Co_xS_2$ system. We shall return to this point later. The assumed linear decrease of the energy gap with temperature has been directly observed in pure NiS_2.[8]

The dependence of γ on x is to be determined by experiment. This assumption of band collapse allows us to distinguish three temperature regimes. At low T (i.e., $kT \ll U$), the bands are well separated, and electrical conduction is dominated by a small, fixed number of holes in the lower band. For higher T (i.e., $kT \approx 0.1\,U$), the number of carriers in both bands increases roughly proportional to $\exp(-U/2kT)$; and at $T > T_s = U_0/\gamma k$ (the temperature at which the energy gap is zero), conduction is dominated by a large fixed number of electrons in a single nearly-half-filled narrow band.

B. Electrical conductivity

Bari[34] has carried out a rigorous calculation of the dc conductivity σ for an extrinsic narrow-band semiconductor with bands containing correlated electrons. He found that the number of excited carriers $n(T)$ is given by

$$n(T) = \frac{4\,n_0(T)\exp(E_F/kT)\{1+\exp[(2E_F-U)/kT]\}}{Z^2}, \tag{2}$$

where E_F is the Fermi energy (chemical potential), $n(T)/n_0(T)$ is the fraction of site pairs permitting electron transfer within the pair, and $n_0(T)$ is a slowly varying function of temperature arising from the statistical sum over site configurations. The single-site grand-partition function Z is given by[35]

$$Z = \left[1 + 2\exp\left(\frac{-E_0+E_F}{kT}\right) + \exp\left(\frac{-2E_0-U+2E_F}{kT}\right)\right]^{N_0}, \tag{3}$$

where E_0 is the energy of an electron on a singly occupied atom and N_0 is the number of independent atomic sites. The Fermi energy E_F and, therefore, Z, depend explicitly on the average site occupancy, and hence, on the cobalt concentration x as given by

$$\exp\left(\frac{E_F-U}{kT}\right) = \frac{-x+[x^2+(1-x^2)\exp(-U/kT)]^{1/2}}{1+x}. \tag{4}$$

Assuming that the carriers form small polarons, we can introduce a temperature-dependent mobility $\mu(T)$,

$$\mu(T) = \mu_0(T)\exp(-E_H/kT),$$

where E_H is half the polaron binding energy and $\mu_0(T)$ is a slowly varying function of temperature.

The conductivity σ is given by $\sigma(T) = n(T)\,e\mu(T)$. In Fig. 11, we demonstrate on the basis of this model the general behavior of $n(T)$, $\mu(T)$, and $\sigma(T)$ as functions of inverse temperature for values of x, U_0, γ, and E_H typical of those deduced from the experimental results. In the resulting plot of $\ln[n(T)]$ vs $1/T$, Fig. 11(a), we observe three temperature regimes. At low and high temperatures, the carrier density is approximately constant, while in the intermediate temperature range it is temperature activated. The existence of three regimes can be understood as follows: At low T (i.e., $kT \ll U$), the Fermi level E_F is in the lower band, and the carrier density is fixed by the intrinsic hole concentration. At intermediate temperatures, E_F rises into the band gap, and at high temperatures, the band gap collapses and E_F moves below the resulting single band. [Since this band is still narrow and less than half-filled, E_F must fall below the band in order that the Fermi function $f(E)$ be less than $\frac{1}{2}$.] For all temperatures, $n(T)$ is an increasing function of x, because the number of carriers increases with

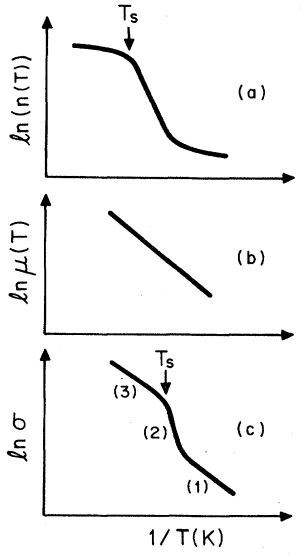

FIG. 11. (a) Number of excited carriers on a ln plot vs inverse temperature for $x = 0.08$, $U_0 = 60$ meV, $\gamma = 3.0$, $E_H = 20$ meV. T_s is the temperature of band collapse. (b) Hopping mobility on an ln plot vs inverse temperature. The slope is E_H, the hopping energy. (c) Conductivity on an ln plot vs inverse temperature. The slopes of the curve are E_H for regions (1) and (3) and $\simeq E_H + \frac{1}{2}U_0$ for region (2).

x. In Fig. 11(a), T_s denotes the temperature of band gap collapse. Figure 11(b) is consistent with a temperature-activated mobility, the carriers forming small polarons of constant activation energy at all temperatures of interest. The resulting temperature-dependent conductivity σ is the product of the curves in Figs. 11(a) and 11(b) and is shown in Fig. 11(c).

C. Thermoelectric power

The thermoelectric power S is the ratio of the effective electric field to the thermal gradient that produces this electric field at zero net electric current. The thermoelectric power of a Hubbard insulator has been calculated by Bari[34] and by Beni.[36] For the case of hopping conduction, we must add to their expressions, a temperature-independent contribution of the form $-k\eta/e$, where $k\eta$ is the change in entropy of an ion due to the presence of an electron.[37] The total thermoelectric power S is then given by

$$S=-\frac{1}{eT}\left(\frac{U}{1+\exp[(U-2E_F)/kT]}-E_F\right)-\frac{k\eta}{e}. \tag{5}$$

Figure 12 shows a representation of the thermoelectric power versus temperature expressed by Eq. (5) for $\eta=0$. For a range of values for x and U typical of those inferred from the experimental results, we find that S falls from a high positive value at low temperatures to a relatively small negative temperature-independent value at high temperatures. For small x so that $x^2 \ll e^{-U/kT}$, and for $\eta=0$, S takes the form[34]

$$S=(-kx/e)[\exp(U/2kT)+1](1-U/2kT). \tag{6}$$

Thus, $S=0$ at $T_0=U/2k=U_0/k(2+\gamma)$. Therefore, our model for $Ni_{1-x}Co_xS_2$ predicts that at low T ($kT \ll U$), the thermoelectric power is large and positive because the conduction is dominated by the small number of holes in the lower band; at high T, the bands have collapsed, and the small, negative temperature-independent thermoelectric power seen in this regime is due to the electrons in the single, nearly half-filled narrow band. The positive peak value of S decreases with x because $S \sim E_F/T$ and E_F decreases as x increases [see Eq. (4)].

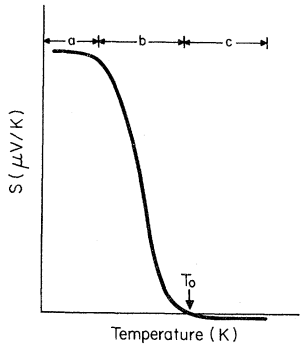

FIG. 12. Theoretical thermoelectric power S vs temperature for $x \simeq 0.03$, $U_0=200$ meV, $\eta=0$. T_0 is the crossover temperature. The low-, intermediate-, and high-temperature regimes corresponding to activation energies E_1, E_2, and E_3 are denoted by the letters a, b, and c, respectively.

V. APPLICATION OF MODEL TO EXPERIMENTAL DATA AND DISCUSSION OF RESULTS

Using the expressions described above, we have generated theoretical curves for σ and S, and thus have obtained values for the electronic parameters contained in the model. The results of the theoretical fits, applying the above model to our experimental data, are shown as the solid curves in Figs. 3–5 and Figs. 6–8. For the corresponding temperature regimes of the experimental data (Figs. 3 and 4) and of the theoretical σ (Fig. 11), the activation energies are denoted by the same subscripts 1, 2, and 3. The low-, intermediate-, and high-temperature regimes of the S data (Figs. 6–8) correspond, respectively, to those labeled by the letters a, b, and c in the theoretical curve of Fig. 12, and to the regimes 1, 2, and 3 of σ.

In fitting the curves, x (for all $x \geq 0.005$) was taken to be the experimentally determined cobalt concentration of the given sample. For each of these values of x, the parameters U_0, γ, and E_H were chosen to optimize the fit to the conductivity data. The energy E_H is given directly by E_1, the low-temperature slope of the conductivity curve. The parameter U_0 is obtained by fitting the σ data in the intermediate-temperature range ($E_2 \sim \frac{1}{2}U_0 + E_H$). The parameter γ is found from the relation $T_s=U_0/\gamma k$. For the values of x where the saturation feature is not observed, T_s is assumed to be greater than 600 K. For a given x, the thermoelectric power curves were fit with the *same* values of U_0 and γ as had been chosen to fit the conductivity curves (S does not depend on E_H). Approximate values for $\mu_0(T=\infty)$ and η, respectively, were then obtained by matching the absolute magnitudes of the theoretical and experimental σ and S plots.

As discussed earlier, the conductivities of the samples with $x \leq 0.005$ fall on a nearly common $\ln\sigma$-vs-$1/T$ curve. This result suggests that for values of x less than the defect concentration, the Co compensates for a corresponding fraction of defects, and the expected results of increasing the Co doping are not observed. As a result, we have chosen for these samples an "effective x,"

$\hat{x}$ ($\hat{x}=0.005$), where the $\hat{x}$ is identified with holes in the lower Hubbard band, but these holes now result from defects as well as Co substitution. Without a detailed knowledge of the defects, the choice of $\hat{x}$ is somewhat arbitrary. To restrict this freedom, we have required that $U_0(x=0.005)$ fall on a smooth extrapolation of the function $U_0(x)$ determined for $x>0.005$. Further, we have required that $E_H(x=0.005)$ and $\gamma(x=0.005)$ be the values of these functions predicted by linear least-squares fits to their values for larger x. (See Sec. V C and Fig. 13.)

A. Comparison of theoretical calculation with conductivity data

Here we compare the results of the calculations with the actual measurements, in order to determine if the model can be applied to the $Ni_{1-x}Co_xS_2$ system. As can be seen in Figs. 3 and 4, the model reproduces well the decrease in the range of values spanned by the conductivity as x increases from 0 to 0.12. This span in σ values is *independent* of the values of the adjustable parameters. The model further explains the anomalous equal activation energies ($E_1=E_3$) observed for $0.05\leq x\leq 0.12$ at low and high temperatures. (For $x<0.05$, the high-temperature regime with activation energy E_3 occurs for $T>600$ K, and therefore was not observable experimentally.) The high-temperature "saturation" points of the conductivity data in the range $0.05\leq x\leq 0.12$ are well fit. For

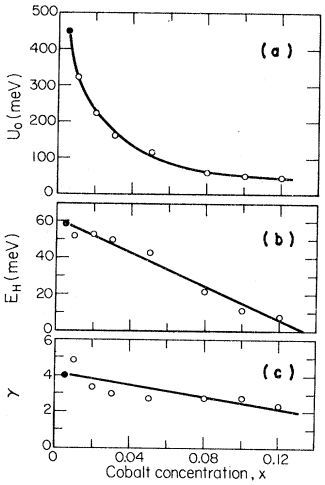

FIG. 13. Parameters used to fit the electrical conductivity and thermopower data for $x\geq 0.01$ are represented by the open circles. The closed circles indicate the values used for $\hat{x}=0.005$ (see Sec. V). (a) Zero-temperature band gap U_0. The solid line is a smooth curve through the points for $x\geq 0.01$. (b) Polaron hopping energy E_H. (c) Temperature coefficient of band collapse, γ. The solid line in (b) and (c) are linear least-squares fits to the points for $x\geq 0.01$.

$x\geq 0.05$, the high temperature ($T\gtrsim 500$ K, corresponding to activation energy E_4) experimental conductivity data suggest that perhaps the effect of the higher-lying antibonding band is becoming important. The model does not attempt to explain the conductivity at this temperature extreme for the values of x exhibiting such deviations. For NiS_2 the theory (Fig. 4) also accounts for the kink in the conductivity data at $T\sim 380$ K discussed earlier. However, at low temperatures ($T\lesssim 100$ K), the theoretical fit deviates from the conductivity data for $x<0.05$. The probable explanation of this is that at such low temperatures, the energies available for single-phonon excitation are inadequate for hopping, so that more than one phonon is needed.[38] The predominance of these multiple-phonon processes results in the disappearance of a well-defined activation energy in this region. No evidence of polaron band conduction was obtained above 77 K, the lowest temperature investigated.

B. Comparison of theoretical calcuation with thermoelectric-power data

A comparison of the predictions of the model with the experimental thermoelectric power data is shown in Figs. 6–8. In general, the theory successfully predicts the x dependence of the peak values in S, the temperature where S peaks, the crossover temperature, and the magnitude of S in the high-temperature limit. In fact, one of the most important successes of the model is that it explains the small, negative, temperature-independent thermoelectric power determined primarily by the entropy term, $k\eta/e$ and observed at high temperatures for $0.005\leq x\leq 0.12$. The values of η obtained for the fit are very close to 0.2, previously suggested by Austin and Mott[39] for small-polaron hopping.

For pure stoichiometric NiS_2, the lower Hubbard-split e_g band would be full and the theory predicts a zero value of the thermoelectric power for all temperatures. However, it has not yet proved possible to grow pure, stoichiometric NiS_2. Consequently, we have used the values of $\hat{x}$ ($\hat{x}=0.005$), U_0, and γ which were determined by our analysis of the electrical conductivity data to evaluate the temperature dependence of the thermoelectric power for small Co concentrations. This is shown as the solid curve in Fig. 7. As is evident, the agreement is good for all $x<0.01$ at temperatures above 250 K. At lower temperatures, the thermoelectric power falls rapidly with decreasing temperature. In this regime, conduction occurs at the Fermi level, which lies near the top of the lower band. The large negative value of $[d\ln g(E)/dE]_{E=E_F}$, where $g(E)$ is the density of states, accounts for this behavior of the thermoelectric power. This

regime is outside the range of validity of our calculations, because at such low temperatures the assumption that the effective bandwidth, Δ, is less than kT no longer holds. The effects of finite bandwidths are expected to be more important for larger values of x, since the zero-temperature bandwidth increases with x. The poor fit at such low temperatures for $x \gtrsim 0.05$ is clearly illustrated in Fig. 8 for $x = 0.10$, where the experimental thermoelectric power data has a temperature-independent value of -38 μV/K for $T > 100$ K, and the theoretical curve deviates from the data below ≈ 250 K, where the curve rises to ≈ 10 μV/K at 100 K. In this case, it is evident that the model does not apply in the low-temperature regime, as we would expect.

In summary, as discussed in Sec. V A, the model provides an explanation for the anomalous features in the observed dependences of the conductivity on temperature and Co concentration. To check various aspects of the model, calculations of the thermoelectric power were made using the same set of parameters that were used for the conductivity and these were in agreement with the data in the temperature range where the assumption that $kT > \Delta$ is valid. This application of the model explains in a natural way those aspects of the thermoelectric-power data which are difficult to explain on the basis of conventional one-electron band models. The quantitative fit to the S vs T data could no doubt be improved by refining the theory to include finite bandwidth effects, but this would introduce another parameter and make the calculations much more complex. In Sec. V C, we discuss the plausibility of the values of the parameters actually used, and show that the optical data support these and other aspects of the model.

C. Discussion of the physical parameters

Additional support for the model comes from the fact that the values used for the parameters U_0, E_H, and γ are consistent with results of both previous studies and the optical experiments performed in the present work. In addition, the infinite-temperature mobilities vary from about 1 cm^2/V sec for the $x = 0.005$ sample to about 5 cm^2/V sec for $x = 0.12$, and $\mu_0(x)$ increases with increasing x. This trend is consistent with the increasing bandwidth as a function of increasing Co concentration. The magnitudes for $\mu_0(x)$ are reasonable for such d-electron materials[32,40] and are also consistent with the results of our Hall measurements. The actual values of the carrier mobilities are always considerably less than 5 cm^2/V sec, and are thus consistent with small-polaron transport.

The dependence of these parameters on cobalt concentration x as shown in Fig. 13, indicates that their values are smoothly decreasing functions of x. As discussed earlier, the straight lines drawn in Figs. 13(b) and 13(c) are least-squares fits to the values of E_H and γ chosen for $x \geq 0.01$ and were used to determine these parameters for $\hat{x} = 0.005$. Because the extension of the smooth curve in Fig. 13(a) was somewhat arbitrary, we chose the value which provided the best fit to the conductivity data. This choice is in reasonable agreement with the optical absorption results presented below. Our value of U_0 for $\hat{x} = 0.005$, $U_0 = 450$ meV, differs from that obtained by Kautz *et al.*[8] for nominally pure NiS_2, $U_0 = 370$ meV, due to a different interpretation of the absorption data as discussed in the next section. Because we cannot calculate U_0 from first principles, we have no independent corroboration of the extrapolated value of U_0 for pure, stoichiometric NiS_2. The zero-temperature gap U_0 and hopping energy E_H vary, respectively, from 450 and 59 meV at $x = 0.005$ to 45 and 8 meV at $x = 0.12$. A decrease in energy gap with x is consistent with the optical-absorption results for $0 \leq x \leq 0.01$, as will be discussed later. The value of the hopping energy $E_H \lesssim 60$ meV is reasonable for small polarons in transition-metal compounds.[40] However, E_H varies by a factor of ~6 from $x \approx 0$ to $x = 0.12$. The systematic decrease in E_H with increasing cobalt concentration is most likely a result of the concomittant increase in zero-temperature bandwidth resulting from the decrease in lattice parameter. It is interesting to note that the linear fit to the values of E_H, shown in Fig. 13(b), extrapolates to zero hopping energy at $x \sim 0.13$. Preliminary studies of the conductivity of samples with $x > 0.12$ suggests that this is, in fact, the case.[41]

The temperature coefficient of band gap collapse γ ranges between $2.6 \leq \gamma \leq 4.0$ for $0 < x < 0.12$ [Fig. 13(c)]. These values are consistent with the results of our optical measurements, described in the following. The optical reflectivity, R, of $Ni_{1-x}Co_xS_2$, measured at room temperature over a photon energy range $0.06 < \hbar\omega < 2$ eV for $x = 0$, and $0.06 < \hbar\omega < 0.5$ eV for $x = 0.01$ and 0.02, is essentially constant at $R = 49\%$ for $x = 0$, $R = 51\%$ for $x = 0.01$, and $R = 70\%$ for $x = 0.02$ over these frequency ranges. However, the results of optical-absorption measurements for the $x = 0.0$, 0.005, and 0.01 samples at $T = 300$, 195, and 77 K, reveal an absorption edge as shown in Fig. 14. Due to the small size of the samples, their large absorption coefficients α and the increase of α with increasing x, it was possible to make optical-absorption measurements only on samples with $x \leq 0.01$.

Unfortunately, because the optical-absorption measurements were very difficult to make, we

could not determine precisely the absorption edge by using any of the conventional procedures described in the literature.[42] From the conductivity fit, the value of 0.34 eV was obtained for the room temperature gap for nominally pure NiS_2. In Fig. 14, we see that this value falls within the energy range where we can reasonably expect the gap to lie. Our optical data agree well with those obtained by Kautz *et al.*[8] (for those photon energies where our measurements overlap). A precise determination of the gap is very dependent on the detailed interpretation of the edge. For example, using a power-law fit to the absorption edge for NiS_2 at room temperature, Kautz *et al.*[8] found a gap of 0.265 eV, in contrast to our value of 0.34 eV. This difference is reflected in the discrepancy in U_0 values, the zero-temperature extrapolations of the gap. Ordinarily, the absorption data could be used to determine the form of the edge, and thus a more definite value for the gap. However, our data are for values of $\alpha < 5\times10^3$ cm^{-1} only, and it is thus very difficult to estimate the functional dependence of the edge, especially since the material contains extensive defects. However, the temperature dependence of the gap can be evaluated much more accurately than the absolute value at any particular temperature. The experimental values thus obtained for γ for $0.0 \leq x \leq 0.01$ are given in Table III. As can be seen, they are in general agreement with those obtained from our analysis of the electrical-conductivity data. The value of $\partial E_g/\partial T = -2.9\times10^{-4}$ eV/K for pure NiS_2 is to be compared with that of -3.9×10^{-4} eV/K reported by Kautz *et al.*[8] Figure 14 also shows that the energy corresponding to the onset of interband absorption shifts to lower energies with increasing x. This indicates that the energy gap decreases with increasing x, consistent with the theory.

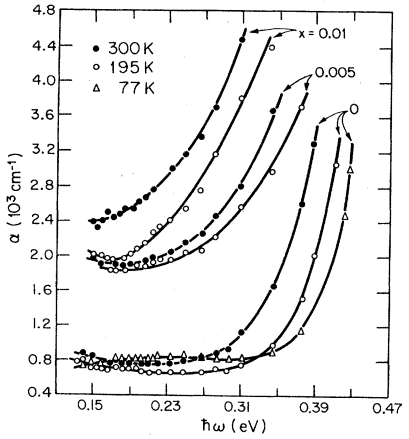

FIG. 14. Absorption coefficient α vs photon energy $\hbar\omega$ for $Ni_{1-x}Co_xS_2$, $x \leq 0.01$ at various temperatures.

D. Discussion of the other experimental results

1. Hall effect

The estimated upper limit of the Hall mobility for the $Ni_{1-x}Co_xS_2$ samples is 0.5 cm^2/V sec. This low value of the Hall mobility is consistent with the predominance of small-polaron hopping conduction in the temperature range investigated. Since the temperature dependence and magnitude of the Hall mobility for small polarons may differ substantially from that of the conductivity mobility,[38] we cannot make a direct comparison between the results of our Hall measurements and the values of the conductivity mobility obtained from the model.

2. Optical absorption and reflectivity

The reflectivity is high (~50% for $x = 0.01$) and constant over the measured frequency ranges. The absence of structure in the reflectivity spectrum in the energy ranges near the absorption edge may be due to the presence of weak oscillators[23] associated with e_g-e_g optical transitions (from the lower to the upper Hubbard bands) which are *not* dipole allowed. The observed absorption edge and the relatively large values of the reflectivity are most likely due to a small admixture of the sulfur p bands into the metallic e_g bands in NiS_2, resulting in a weak matrix element for optical transitions between the bands. In order to estimate the degree of covalent mixing in the e_g bands, it is convenient to discuss the effective number of electrons per atom n_{eff}, contributing to the optical properties over a finite frequency range as defined by the sum rule[43]

$$\int_0^{\omega_c} \omega\epsilon_2(\omega)\, d\omega = \frac{2\pi^2 N e^2}{m} n_{\text{eff}}(\omega_c), \tag{7}$$

where $\epsilon_2(\omega)$ is the imaginary part of the dielectric function, ω_c is the upper frequency of interest and N is the number of molecules per unit volume. The sum rule [Eq. (7)] shows that

$$\lim_{\omega_c \to \infty} n_{\text{eff}}(\omega_c) = n,$$

TABLE III. Estimated values of the temperature coefficient of the energy gap for $Ni_{1-x}Co_xS_2$, $x \leq 0.01$. Values of γ obtained from the fits to the electrical conductivity and those obtained from the optical absorption experiments are shown. Temperature derivatives of the gap are calculated from γ using the relation $E_g = E_g^0 - \gamma kT$.

Cobalt concentration x	Conductivity γ	Optical absorption γ	Optical absorption $\frac{\partial E_g}{\partial T}$ (10^{-4} eV/K)
0.0	4.1	3.4	−2.9
0.005	4.1	3.5	−3.0
0.01	4.9	4.4	−3.8

where n is the total number of electrons per molecule.[43]

Using Eq. (7) and the measured values of the optical absorption coefficient and reflectivity for NiS_2 at room temperature, we obtain $n_{\text{eff}} \simeq 2\times10^{-3}$ for $\omega_c = 0.41$ eV. Since 0.41 eV is greater than the separation between the e_g bands (the model predicts a room-temperature gap of 0.34 eV), we should obtain a value of $n_{\text{eff}} = 2$, for an oscillator strength of 1. Thus, the very small value of n_{eff} obtained implies a very small oscillator strength for the e_g-e_g optical transitions. Consequently, the widths of the metallic $3d$ bands, which are determined by the degree of mixing with sulfur $3p$ states, may be quite small. The width of the e_g band has been a source of controversy in transition metal compounds.[6,32] We have been unable to understand the data presented in this paper with a wide-band model. As mentioned previously, the gradual as opposed to abrupt decrease in the size of the energy gap with increasing temperature also suggests narrow bandwidths. We can conclude that these considerations provide strong evidence that transport in the $Ni_{1-x}Co_xS_2$ system takes place in a narrow band, independent of the validity of the specific model presented here. However, the assumption of small-polaron formation and the concommitant effective band narrowing with increasing temperature provides a simple resolution of the bandwidth problem in these materials in general.[44] But, in particular, since such an assumption yields good agreement between theory and experiment for the $Ni_{1-x}Co_xS_2$ system, we feel strongly that small-polaron formation is at present the most likely explanation of transport in this class of materials.

VI. CONCLUSIONS

We have presented the results of measurements of electrical conductivity, thermoelectric power, Hall effect, optical absorption, and reflectivity in single crystals of the system $Ni_{1-x}Co_xS_2$, for $0 \leq x \leq 0.12$. The results of the conductivity and the thermoelectric-power measurements exhibit anomalous properties which cannot be accounted for in terms of conventional one-electron band theory. However, we have shown that these results may be explained by a model which involves small-polaron hopping conduction in a narrow correlation split band. This study of the composite system, $Ni_{1-x}Co_xS_2$ thus strongly suggests that NiS_2 is a Mott insulator. The extension of this model to other systems, $Ni_{1-x}Co_xS_2$ for $x > 0.12$, $Ni_{1-z}Cu_zS_2$, and $NiS_{2-y}Se_y$ is presently under investigation and will be reported elsewhere.[45]

ACKNOWLEDGMENTS

We wish to thank M. Finn, I. Mroczksowski, and E. Owens of the MIT Lincoln Laboratories for their electron microprobe analysis, x-ray fluorescence measurements, and chemical analysis. We also gratefully acknowledge the technical assistance of Dr. J. Kalnajs, Dr. D. Gabbe, and Dr. A. Linz of the MIT Center for Materials Science and Engineering Crystal Physics Laboratory for the growth of the single crystal materials; and the technical assistance of A. Colozzi of the MIT Electrical Engineering and Computer Sciences Department, and of L. Rubin of the Francis Bitter National Magnet Laboratory. This work was supported by National Science Foundation–Materials Research Laboratory Grant No. DMR 76-80895.

---

*Department of Physics.
†Present address: University of Benin, Nigeria.
‡Present address: T. J. Watson Research Center, Yorktown Heights, N. Y. 10598.
§Department of Electrical Engineering and Computer Science.
‖Present address: Department of Physics, University of Kentucky, Lexington, KY 40506.

[1]T. A. Bither, R. J. Bouchard, W. H. Cloud, P. C. Donohue, and W. J. Siemons, Inorg. Chem. 7, 2208 (1968).
[2]H. S. Jarrett, W. H. Cloud, R. J. Bouchard, S. R. Butler, C. G. Frederick, and J. L. Gillson, Phys. Rev. Lett. 21, 617 (1968).
[3]J. B. Goodenough, J. Solid State Chem. 5, 144 (1972); 3, 26 (1971).
[4]S. Ogawa, S. Waki, and T. Teranishi, Int. J. Magn. 5, 349 (1974).
[5]J. A. Wilson and A. D. Yoffe, Adv. Phys. 18, 193 (1969).
[6]J. A. Wilson, Adv. Phys. 21, 143 (1972); J. A. Wilson, in Proceedings of the Conference on Phase Transitions and Their Applications in Materials Science, University Park, Pennsylvania, 1973 (unpublished), p. 101.
[7]J. A. Wilson and G. D. Pitt, Philos. Mag. 23, 1297 (1971).
[8]R. L. Kautz, M. S. Dresselhaus, D. Adler, and A. Linz, in *Proceedings of the Eleventh International Conference on the Physics of Semiconductors* (PWN-Polish Scientific, Warsaw, 1972), p. 807.
[9]S. Endo, T. Mitsui, and T. Miyadai, Phys. Lett. 46A, 29 (1973).
[10]G. Krill, M. F. Lapierre, F. Gautier, C. Robert, G. Czjzek, J. Fink, and H. Schmidt, J. Phys. C 9, 761 (1976).
[11]F. Gautier, G. Krill, M. F. Lapierre, and C. Robert, Solid State Commun. 11, 1201 (1972).
[12]R. J. Bouchard, J. L. Gillson, and H. S. Jarrett, Mater. Res. Bull. 8, 489 (1973).
[13]J. Hubbard, Proc. R. Soc. London Ser. A 276, 238 (1963).

[14]A. K. Mabatah, E. J. Yoffa, P. C. Eklund, M. S. Dresselhaus, and D. Adler, Phys. Rev. Lett. 39, 494 (1977).
[15]R. J. Bouchard, J. Cryst. Growth 2, 40 (1968).
[16]Specpure nickel and sulfur powders were obtained from Johnson and Matthey Chemicals.
[17]Reagent-grade nickel-sulfate crystals and cobalt-sulfate crystals were used.
[18]R. J. Bouchard, Mater. Res. Bull. 3, 563 (1968).
[19]S. R. Butler and R. J. Bouchard, J. Cryst. Growth 10, 163 (1971).
[20]The chemical analysis and x-ray fluorescence measurements were done by I. Mroczkowski and E. Owens of MIT Lincoln Laboratory.
[21]L. J. Van der Pauw, Philips Res. Rep. 13, 1 (1958).
[22]The Hall-effect measurements were made using magnetic fields at the Francis Bitter National Magnet Laboratory.
[23]A. K. Mabatah, Ph.D. thesis (Massachusetts Institute of Technology, 1977) (unpublished).
[24]P. C. Eklund and A. K. Mabatah, Rev. Sci. Instrum. 48, 775 (1977).
[25]Vacuum grease made by Dow Corning (Catalog No. 970V).
[26]S. Furuseth, A. Kjekshus, and A. F. Andersen, Acta Chem. Scand. 23, 2325 (1969).
[27]J. M. Honig (private communication).
[28]W. Z. Biltz, Anorg. Allgem. Chem. 228, 275 (1936).
[29]M. A. Khan, J. Phys. C 9, 81 (1976).
[30]E. K. Li, K. H. Johnson, D. E. Eastman, and J. L. Freeouf, Phys. Rev. Lett. 32, 470 (1974); A. Ohsawa, H. Yamamoto, and H. Watanabe, J. Phys. Soc. Jpn. 37, 568 (1974).
[31]T. Holstein, Ann. Phys. (N.Y.) 8, 343 (1959).
[32]D. Adler and J. Feinleib, Phys. Rev. B 2, 3112 (1970).
[33]E. J. Yoffa and David Adler, Phys. Rev. B 20, 4044 (1979).
[34]R. A. Bari, Phys. Rev. B 10, 1560 (1974).
[35]E. J. Yoffa and D. Adler, Phys. Rev. B 12, 2260 (1975).
[36]G. Beni, Phys. Rev. B 10, 2186 (1974).
[37]R. R. Heikes, in *Thermoelectricity*, edited by R. R. Heikes and W. U. Ure (Interscience, New York, 1961), Chap. IV.
[38]D. Emin, J. Solid State Chem. 12, 246 (1975).
[39]I. G. Austin and N. F. Mott, Adv. Phys. 18, 41 (1969).
[40]D. Adler, Solid State Phys. 21, 1 (1968).
[41]E. J. Yoffa, A. K. Mabatah, P. C. Eklund, D. Adler, and M. S. Dresselhaus, Inst. Phys. Conf. Ser. 43, 473 (1979).
[42]For example, see T. S. Moss, *Optical Properties of Semiconductors* (Butterworths, London, 1959), Chap. 2.
[43]For example, see F. Wooten, *Optical Properties of Solids* (Academic, New York, 1972), Chap. 3.
[44]D. Adler, in *Handbook of Semiconductors*, edited by W. Paul (North-Holland, Amsterdam, 1980), Vol. 1, in press.
[45]P. Kwizera, M. S. Dresselhaus, and David Adler, Phys. Rev. B (to be published).